Tailored Waveform of Dielectric Barrier Discharge to Control Composite Thin Film Morphology

Paul Brunet[1,2], Rocío Rincón[2], Zineb Matouk[2], Mohamed Chaker[2*] and Françoise Massines[1*]

1) Laboratoire PROcédés Matériaux et Energie Solaire, UPR 8521, Tecnosud, 66100 Perpignan, France

E-mail: francoise.massines@promes.cnrs.fr

2) Institut National de la Recherche Scientifique, 1650 boulevard Lionel Boulet Varennes, Québec, Canada, J3X1S2

E-mail: chaker@emt.inrs.ca

ABSTRACT

Nanocomposite thin films of TiO_2 in a polymer-like matrix are grown in a filamentary Argon (Ar) Dielectric Barrier Discharge (DBD) from a suspension of TiO_2 nanoparticles in isopropanol (IPA). The sinusoidal voltage producing the plasma is designed to independently control the

matrix growth rate and the transport of nanoparticles (NPs) aggregates to the surface. The useful FSK (Frequency Shift Keying) modulation mode is chosen to successively generate two sinusoidal voltages: a high frequency of 15 kHz and a low frequency ranging from 0.5 to 3 kHz. The coating surface coverage by the NPs and the thickness of the matrix are measured as a function of the FSK parameters (the duty cycle between these two signals is varied from 0% to 100% and the low frequency). It is observed that the matrix thickness is mainly controlled by the power of the discharge which largely depends on the high frequency value. The quantity of NPs deposited in the composite thin film is proportional to the duration of the low frequency applied. The FSK waveform has a double modulation effect allowing to obtain uniform coating as the NPs are not affected by the high frequency and the matrix growth rate is limited when the low frequency is applied. When it is close to a frequency limit, the low frequency acts like a filter for the NPs aggregates. The higher is the frequency, the smaller is the size of the aggregates transferred to the surface. By only changing the FSK modulation parameters, the thin film can be switched from superhydrophobic to superhydrophilic and in suitable conditions, a nanocomposite thin film is obtained.

1. INTRODUCTION

Since the last decade, aerosol assisted chemical vapor deposition[1] using atmospheric pressure plasmas has been studied to develop a one-step method for the deposition of thin film[2] or nanocomposite thin films[3]. Nanoparticles (NPs) in suspension in a polymerizable liquid are sprayed in a Dielectric Barrier Discharge (DBD). With this method, anticorrosive,[3] superhydrophobic,[4, 5] self-cleaning or super hydrophilic thin films[6, 7] were successfully grown. In any case, the gas and the precursors are injected at one plasma end and the effluents are extracted at the other end.

Previous works have shown that homogenous coatings can be obtained thanks to either plasma modulation or using well-suited process conditions. In particular, it was demonstrated that a Scott chamber connected to the nebulizer makes the aerosol more suitable than a cyclonic chamber.[8] In nitrogen, keeping the discharge homogenous and using a specific waveform combining two frequencies is helpful to achieve a well-controlled and uniform nanocomposite thin film.[9] However the control of the density of NPs is not yet achieved.

The aim of the present work is to sequentially produce plasma at two different frequencies to control independently the transport of the NPs and the matrix growth rate. This approach results from two previous observations. From a former work, NPs are only deposited for frequencies typically lower than 1 kHz while the matrix growth rate increase with the DBD frequency.[10] First, it is known that in a DBD operated in the kHz-frequency range, the electrostatic force efficiently ensures the transport of NPs towards the surface as far as the NPs diameter is of the order of 20 nm or more and the oscillation frequency of the voltage is low enough.[11, 12] This is explained by the relative amplitude of the different forces acting on a NP in a DBD working in a PECVD configuration. As soon as the NPs reach a radius large enough to result in a fixed electrical charge, the electrostatic force due to the discharge voltage becomes the strongest force. The lower is the frequency of the sinusoidal voltage generating the discharge, the larger is the oscillation amplitude of the NPs[13] and thus the broader is the gas region from which the NPs drift from the bulk to the surface. The amplitude of oscillation becomes significant as compared to a mm gap for frequencies in the kHz range. Second, in a PECVD (Plasma Enhanced Chemical vapor deposition) process, the energetic species produced by the plasma initiate the thin film precursor decomposition. Higher is the plasma power higher is the density of these species. If this density is low compare to the precursor one, the thin film growth rate is limited by the

energetic density and thus by the discharge power. The DBD power relevant for the deposition of films[14] with good quality is rather restricted while the film growth rate increases with the discharge power.[15] As the DBD is pulsed in the range of frequencies considered,[16] the easiest way to increase the power of the DBD is by raising the frequency of the discharge i.e. by increasing the number of events per second. Recent work[10] on composite thin films made from a suspension of 20 nm-diameter TiO_2 NPs in isopropanol (IPA), shows that these features are particularly true for polymer-like thin film grown from IPA in an Ar DBD. More specifically, the frequency should be larger than 10 kHz to ensure a thin film deposition. On the other hand, 10 kHz prevents the drift of TiO_2 NPs to the surface. These results indicate that for precursors made of 20 nm-diameter TiO_2 NPs and IPA, there is a gap between the limit frequencies of the matrix growth (> 10 kHz) and the NPs transport to the surface (< 1 kHz). On the basis of these observations, the objective of the present work is to identify a voltage waveform that exploit this gap between the limit frequencies in order to independently control the drift of the NPs towards the substrate and the polymerization of the liquid vapor. But also to determine the key parameters governing each step of the composite thin film growth. The Frequency Shift Keying modulation (FSK) appears as a good candidate to easily alternate two frequencies. This voltage waveform was developed to modulate digital signals so that they can be transmitted wirelessly. Binary FSK uses two frequencies values to represent a binary value of 1 and 0. The frequency and the duty cycle of the binary signal as well as the frequency associated with either 1 or 0 values is freely chosen and precisely controlled. In this work, FSK modulation is used with one frequency well adapted to the matrix growth and the other well suited for NPs drift toward the surface. The consequence of this double modulation waveform on the morphology of the thin

film coating made from IPA and TiO_2 NPs is studied. Wettability of the surface is also considered.

2. EXPERIMENTAL SETUP AND METHODS

The colloidal suspension of NPs in the matrix precursor is injected in the plasma as an aerosol by an atomizer as described by Fanelli *et al.*.[17] It acts as a filter in size thanks to wall impact effects. The suspension is placed under magnetic stirring all along the experiment to avoid NPs sedimentation. Deposition is performed during 20 min on a silicon substrate placed on the lower electrode. The total flow of Ar is 5 $L.min^{-1}$ (1.1 $L.min^{-1}$ within the atomizer and 3.9 $L.min^{-1}$ for the dilution). The matrix precursor is IPA and the TiO_2 NPs are 20 nm diameter type T805 from Evonik®. There is 1% in weight of TiO_2 in IPA and 0.2 $g.min^{-1}$ is injected in the plasma. The droplets are evaporated before the plasma, which induces the aggregation of TiO_2 NPs enclosed in the same droplet. The size of the NPs aggregates ranges between 100 nm and a few micrometers.

The schematic representation of the discharge cell is presented in Figure 1a. Two plane parallel electrodes, covered by a dielectric layer, are placed into a closed vessel. The substrate is on the lower dielectric. The argon flow containing the TiO_2 NPs aggregates and the IPA vapor is injected into the 2 x 40 mm^2 gap between the substrate and the upper dielectric surface. Once injected, the gas is guided by two quartz bars until its aspiration on the opposite side of the plasma. The gas residence time in the plasma zone is 38 ms. The plasma is generated in the gas gap between the two electrodes covered by a dielectric layer by applying a high amplitude sinusoidal voltage (HV) to the top electrode while the bottom one is grounded. HV is issued from a low frequency signal generator (Agilent 33220) using FSK modulation and an audio

amplifier (Crest CC4000) connected to an up-voltage transformer (Boige et Vignal). The transformer is designed to operate from 1 to 10 kHz with a voltage ranging from 1 to 15 kV.

Figure 1b presents one cycle of a typical FSK high voltage waveform applied to the electrodes. Frequency-Shift Keying is a method for transmitting digital signals. The two binary states, logic 0 (low) and 1 (high), are each represented by an analog waveform. Logic 0 is represented by a wave at a specific frequency and logic 1 is represented by a wave at a different frequency. The FSK waveform is defined by 4 parameters: the FSK frequency ($f_{FSK} = 1/T_{FSK}$), with T_{FSK} the period of the binary signal, the frequency associated with the logic state 1 (f_H) called high frequency, the frequency associated to the logic state 0 (f_L) called the low frequency and their duty cycle (DC) defined as $T_{OnFSK}/(T_{FSK})$: the higher is the DC, the longer is f_H applied.

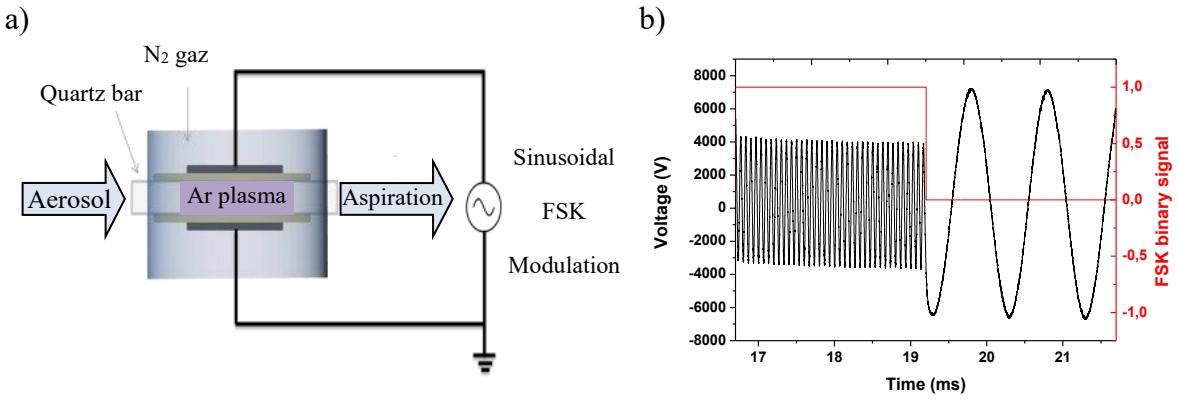

Figure 1: a) Schematic representation of the discharge cell and b) One cycle of a FSK modulation waveform applied onto the electrodes: the FSK frequency (f_{FSK}) is 200 Hz, the high frequency (f_H) is 15 kHz, the low frequency (f_L) is 1 kHz and the duty cycle (DC) is 50%.

The values of the high and the low frequencies were chosen according to a previous study taking into account the possibilities allowed by the experimental set up.[10] On the one hand, our

previous study shows that for given conditions and thin film precursors, the high frequency should be larger than 10 kHz to ensure a thin film deposition from IPA and the low frequency, lower than 1 kHz to ensure an efficient transport of the NPs to the surface. On the other hand, due to the characteristics of the high-voltage transformer, the frequency values allowing to produce a voltage high enough to turn on the plasma lie between 0.5 kHz and 15 kHz. Therefore, the high frequency value is set at 15 kHz while the low frequency is usually set at 1 kHz even though it can be varied from 0.5 to 3 kHz. In all cases, the amplitude of the low frequency voltage is 7 kV while that of the high frequency is 3.5 kV. This difference is due to the high voltage transformer characteristics. The corresponding power of the 15 and 1 kHz discharges is 0.73±0.04 and 0.18±0.03 $W.cm^{-2}$ respectively.

Taking into account the numerous possibilities of the FSK mode, three sets of experimental conditions are considered. They are summarized in Table 1 for the first and the second sets and in Table 2 for the third one:

- For the first set of experiments, the varying parameter is the duty cycle while f_{FSK} is constant and equal to 200 Hz. Five different DCs are used: 0%, 20%, 50%, 80% and 100%. As f_{FSK} is constant, the number of low and high frequency cycles on each FSK cycle changes in an opposite way. T_{FSK} is 5 ms. On average, the precursor undergoes 8 FSK cycles when traveling along the discharge.
- The second set of experiments also compares different DC but the low frequency is always applied over 2.5 ms per FSK cycle. Therefore, to achieve DC values of 40%, 50% and 60% the f_{FSK} and the duration over which the high frequency per FSK cycle, t_{fH}, is applied are changed.

- For the third set of experiments the low frequency value is the varying parameter. It changes from 0.5 kHz to 3 kHz. The DC is set at 20% and f_{FSK} at 200 Hz, which corresponds to duration of 4 and 1 ms over which the low and the high frequencies are applied during one FSK cycle. The number of low frequency cycles per FSK cycle ($N_{Lf\text{-}FSK}$) changes from 2 to 12.

Table 1: First and second sets of values of the different FSK modulation parameters considered in this study (f_H = 15 kHz, f_L = 1 kHz): f_{FSK}: frequency of the binary FSK signal, DC: duty cycle defined as the ratio t_{fH}/T_{FSK} , t_{fH}: duration per FSK cycle other which the high frequency voltage is applied, t_{fL}: duration per FSK cycle other which the low frequency voltage is applied, N_{FSK} : number of FSK periods during the gas mean residence time in the plasma (38 ms), $P_{FSK\text{-}fH}$ and $P_{FSK\text{-}fL}$: power of the high and low frequency discharge taking the modulation into account, P_{FSK} ($P_{FSK\text{-}fH}$+ $P_{FSK\text{-}fL}$): total power and Total N_{fL}: total number of low frequency periods during the precursor mean residence time (38 ms).

	f_{FSK} (Hz)	DC (%)	t_{fH} (ms)	t_{fL} (ms)	N_{FSK}	$P_{FSK\text{-}fH}$ ($W.cm^{-2}$)	$P_{FSK\text{-}fL}$ ($W.cm^{-2}$)	P_{FSK} ($W.cm^{-2}$)	Total N_{fL}
First set	X	0	0	38	X	0	0.19	0.19	38.4
	200	20	1	4	8	0.13	0.12	0.25	30.7
	200	50	2.5	2.5	8	0.35	0.09	0.44	19.25
	200	80	4	1	8	0.59	0.03	0.62	7.7
	X	100	38	0	X	0.80	0	0.8	0

Second set	240	40	1.67	2.5	9.6	0.29	0.11	0.4	16
	200	50	2.5	2.5	8	0.36	0.10	0.46	20
	160	60	3.75	2.5	6.4	0.44	0.07	0.51	24

Table 2: Third set of values for the different FSK modulation parameters (f_H = 15 kHz, f_{FSK} = 200 Hz, DC = 20%, t_{fH} = 1 ms and t_{fL} = 4 ms). With $N_{fL\text{-}FSK}$, the number of periods of low frequency period per FSK cycle, $P_{FSK\text{-}fH}$ and $P_{FSK\text{-}fL}$: power of the high and low frequency discharge taking the modulation into account, P_{FSK} ($P_{FSK\text{-}fH}$+ $P_{FSK\text{-}fL}$): total power and Total N_{fL} corresponding to the total number of low frequency periods during one precursor residence time (38 ms).

	f_L (kHz)	$N_{fL\text{-}FSK}$	$P_{FSK\text{-}fH}$ ($W.cm^{-2}$)	$P_{FSK\text{-}fL}$ ($W.cm^{-2}$)	P_{FSK} ($W.cm^{-2}$)	Total N_{fL}
Third set	0.5	2	0.13	0.06	0.19	15.4
	1	4	0.13	0.12	0.25	30.7
	2	8	0.13	0.24	0.37	61.4
	3	12	0.13	0.36	0.49	92.2

The surface and cross-section morphology of TiO_2 NPs plasma thin films are investigated by Scanning Electron Microscopy (SEM Hitachi S-4500). The images are acquired in the high resolution mode with an extraction voltage of 5 kV and a magnification from ×10 to ×100 K. The surface coverage is measured using ImageJ software by converting the SEM picture into a

binary one. Therefore, the SEM images were converted to black & white images where the white part corresponds to the NPs covering the surface and the black part to the uncovered surface. Then, the surface coverage is defined as the ratio of the white surface to the total surface analyzed. In order to reduce the error, large surfaces of 12 µm x 9 µm were analyzed. For each point, measurements were performed on 3 different locations corresponding to the same gas residence time in the plasma.The chemical composition of the coating is analyzed by X-ray photoelectron spectroscopy (VG Escalab 220i XL) using a 1486.6 eV, Al Kα X-ray source. Survey (0–1400 eV) and high resolution (C1s, O1s, Ti2p) spectra are recorded. The atomic percentage of each element is determined from the high resolution spectra with the CasaXPS software after calibration of the binding energy by using the carbon C1s peak at 285 eV corresponding to the hydrocarbon (C-C/C-H). The diffraction spectra of the thin film is analyzed by X-Ray Diffraction (Panalytical X-Pert PRO MRD), with Cu-KαX-Ray of wavelength (λ) = 1,5406 Å taken from 20 to 80 (2θ degree).

3. RESULTS AND DISCUSSION

3.1 Effect of FSK parameters on the NPs deposition

Figure 2 shows the drastic evolution of the coating morphology for the first set of experiment i.e. with the DC increase and f_{FSK} constant. It presents the 20 min coating deposited on a 2 inches silicon wafer and typical SEM images of the surface and cross-section of the film.

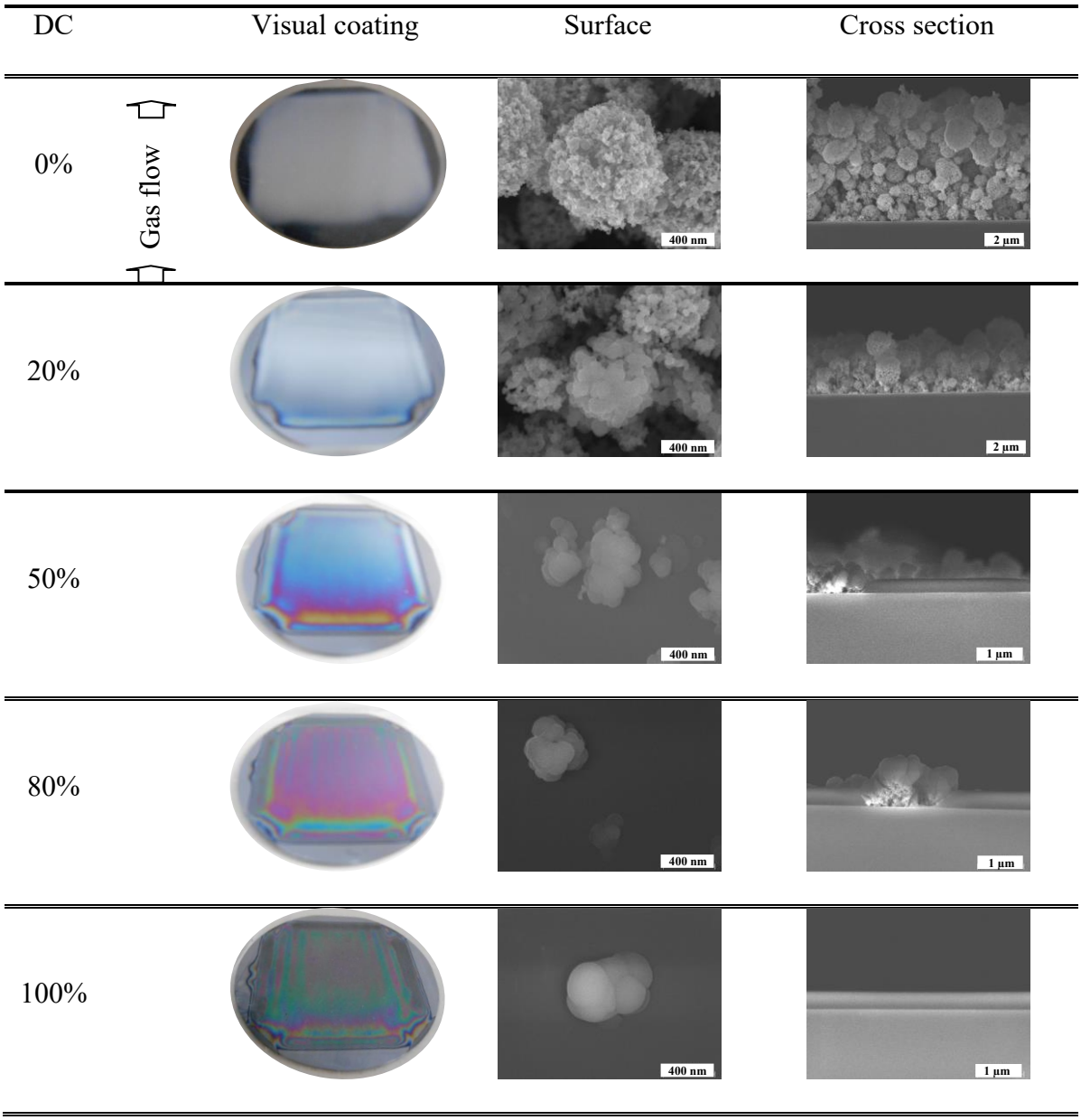

Figure 2: Photographs of the 20 min coating and corresponding SEM images of the surface and cross-section obtained with the first set of parameters: DC of 0%, 20%, 50%, 80% and 100%. The white color is characteristic of the light scattering on the NPs aggregates.

When the DC is equal to 0, i.e. when only f_L is applied, the coating is uniformly white, which indicates the presence of numerous NPs aggregates scattering the light. For a DC of 20% and 50%, the white zone dominates farther from the plasma entrance. For larger DC, the thin film

scatters less and less the light. The SEM images explain these differences. Various structures are observed on the SEM images by increasing the DC, i.e. the duration of the high frequency. When the DC is equal to 0%, a high concentration of NPs aggregates is deposited over the whole substrate. The initial 20 nm TiO_2 NPs forming the aggregates are easily observed, which shows that they are not covered by a polymer-like coating. When the DC increases, two phenomena occur. First, the NPs agglomerates are more and more coated by the polymerized layer masking the 20 nm initial size of the NPs. The well-defined structure starts to blur for a DC of 20% and it completely vanishes at a DC from 50% and beyond. Second, the NPs concentration decreases. Indeed, the substrate is fully covered by the NPs from the entrance to the exit at 0% and 20% while it is only partially covered at 50% or beyond. This can also be seen in Figure 3 where the percentage of Ti, C and O determined by XPS for a residence time of 20 ms is presented as a function of DC. For DC = 0%, the Ti percentage is high (20%). The percentage of O is slightly higher than double Ti and that of C is close to that of Ti (25%). As DC increases, Ti decreases to reach 0 for DC = 50%. Carbon percentage drastically increases (from 25% to 70%) between DC = 0% and 20%. Oxygen drastically decreases between DC = 0% and 20%. These variations are explained by the increase of the discharge power when the DC increases, leading to an increase of IPA dissociation and of carbon concentration. At the same time, the Ti concentration decreases due to a decrease of the duration over which the low frequency is applied. Above DC = 50%, the Ti concentration cannot be evaluated by XPS due to the coverage of NPs by the polymer like coating.

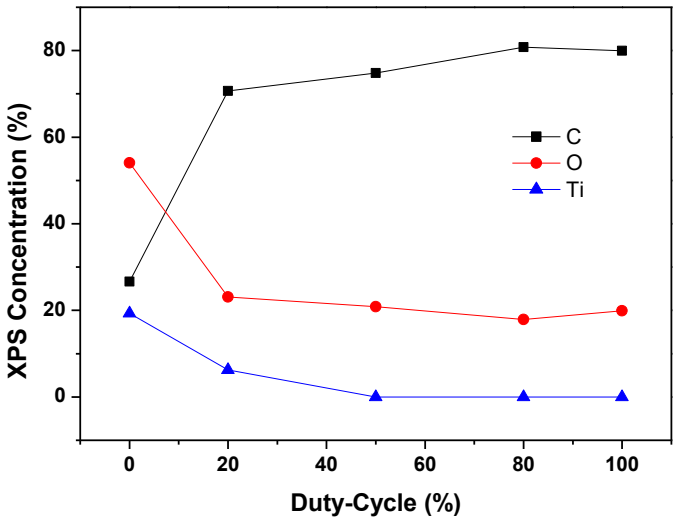

Figure 3: Elementary composition of the thin film measured by XPS as a function of the Duty-cycle (DC). The data correspond to carbon (square), oxygen (circle) and titanium (triangle).

Figure 4 presents the XRD pattern measured for DC=0 and 20%. The main crystalline orientations corresponding to anatase TiO_2 (101-004-200-105-211-204 -220-215) are observed. As expected, the XRD measurements confirm the XPS data since above a DC of 50%, no peak corresponding to TiO_2 NPs is measured and the film is totally amorphous.

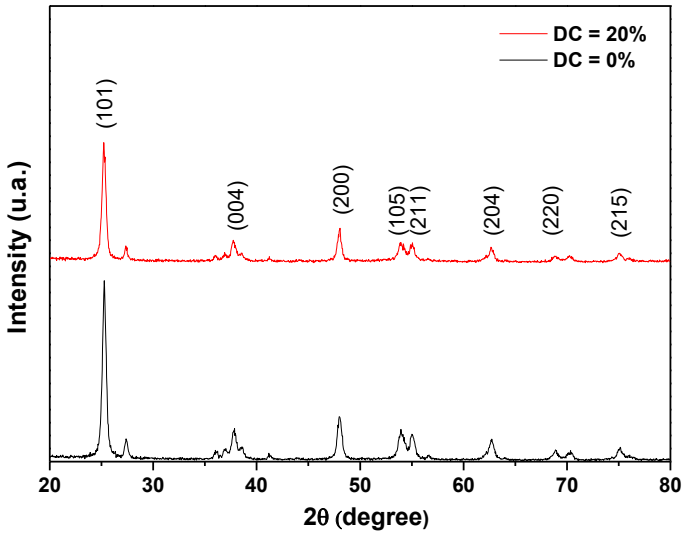

Figure 4: XRD pattern of the thin film for a DC = 0% and DC = 20**%.**

In Figure 5, the average surface coverage of the substrate by the NPs determined from surface SEM images is shown as a function of the duration over which the low frequency is applied to the NPs during their transport in the plasma. The observed correlation is confirmed by the results obtained with the second set of parameters showing that this relationship is independent of the duration of each period of low frequency during one FSK cycle and of the number of times the frequency shift from 15 to 1 kHz during the residence time of NPs in the plasma. This trend is only true for a low frequency of 1 kHz. Result for a lower f_L value, third set, is also reported in Figure 5. For f_L = 0.5 kHz (Third set), 100% of surface coverage is reached for a shorter residence time than for f_L=1 kHz. Lower is the frequency, higher is the oscillation amplitude of the NPs. Larger is the NPs oscillation amplitude, higher is the quantity of nanoparticles deposited during one cycle and shorter is the gas residence time to fully cover the substrate.

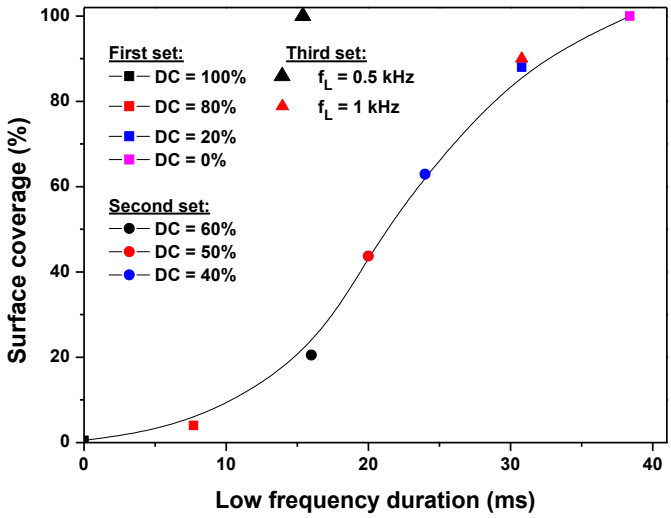

Figure 5: Average surface coverage as a function of the low frequency duration during the residence time of the NPs in the plasma. The data correspond to the first set (square), second set (circle) and third set (triangle) of parameters.

This observation is quite surprising, because after the first half cycle of low frequency, one could expect that the particles that would not have reached the surface yet would oscillate in the gas bulk unless diffusion pushes them towards a surface. Such an event would occur over a time scale of tens of ms and is not very significant at atmospheric pressure. Our observation also contradicts that reported in Profili *et al*[9] where only half a cycle of a 1 kHz voltage is applied to fabricate nanocomposites. In their conditions, the NP oscillation is longer than the gas gap which is half of the one used in the present study. The oscillations are also longer than in our case because the voltage amplitude is larger and the size of the NPs is quite smaller (20 nm compared to about 1 µm in our study). Another difference deals with the discharge regime, namely a diffuse Townsend DBD that simultaneously charges all the NPs in contrast with our discharge, a filamentary discharge, which formed of 100 µm diameter channels that requires several cycles

before the whole volume is filled. In the case of filamentary discharges, it can be assumed that the NPs aggregates are charged only when they lie within a discharge channel so that several cycles are needed to charge all the aggregates. Another mechanism that could contribute is the mutual electrostatic repulsion between the NPs due to the space charge field generated by the accumulation of charged particles.[18] This explains why the parameter controlling the surface coverage by the NPs is the 1 kHz cycle. Moreover, as it is shown in figure 5, for the same power (same energy), the surface coverage is the same within a few percent (less than 3%) between the sets 1 and 3.

Figure 6 shows the water contact angles (WCA) measured on samples made with the first set of conditions as a function of the position in the plasma. For DC = 0% and residence times of 5, 15, 25 ms, the water droplet spreads over the surface. The angle is too small to be measured and it is therefore assumed to be 0°. Furthermore, it is observed that the adhesion of the thin film to the substrate is so low that the water droplet peels the thin film off. For the last position in the plasma corresponding to a residence time of 35 ms, the WCA increases to 150°. For DC=20%, a similar behavior is observed except that the rise from 0° to 150° occurs at the plasma entrance. For DC=50% and DC=80%, a WCA of 100° and 92° is measured respectively, whatever the position and no degradation of the film is observed. This value is that of the hydrophobic polymer-like coating[19] made from IPA (DC=100%). The values vary from 0 to 150°, which means that the surface wettability changes from superhydrophilic to superhydrophobic. These extreme values are observed for the coatings that contain many NPs aggregates (DC = 0 or 20%) inducing a hierarchical nanotexture. According to the literature,[20-23] the surface of a hydrophobic (hydrophilic) material becomes super-hydrophobic (hydrophilic) if it is hierarchical nanotextured. The TiO_2 surface is hydrophilic while that of the polymer like is hydrophobic.

Therefore, the variation from superhydrophilic to superhydrophobic surface, for DC = 0% and 20% is explained by SEM observation and XPS and RDS measurement. According to SEM images, for DC=0%, no polymer like coating is observed on the NPS except at the plasma exit. This is in agreement with XPS and XRD measurements made for a residence time of 20 ms: for DC = 0%, there is 20% of Ti and only 25% of C and for DC = 20%, the Ti percentage is decreased by a factor higher than 3 while that of C is multiplied by a factor 3. In the two cases, the surface is hierarchically nanostructured but in one case it is mainly a TiO_2 surface i.e. a hydrophilic surface while in the other case it is mainly a polymer like surface i.e. an hydrophobic surface. For DC = 0%, the low frequency is only applied. In that case, the power is low. The IPA is very slowly activated and a long interaction with the plasma is needed to allow the polymer to be deposited on the NPs. This explains why it is only observed at the plasma exit. By increasing DC value the power of the discharge increases, due to the time allowed to the high frequency, the precursor can be deposited closer to the entrance. For DC = 20%, the aggregates are polymer-like coated except at the plasma entrance where they are deposited before to interact with the high frequency discharge i.e. before to be coated with polymer, in agreement with the low WCA values. For DC = 0% and 20% Wetting Transition from the Cassie–Baxter State to the Wenzel State is observed and related to the transition in the chemical composition of the surface from $Ti0_2$ to CH. For higher DC values, the transfer of NPs to the surface decreases and the hierarchical structure tends to vanish leading to a WCA closer to that obtained for the film made from IPA alone.. In conclusion, the water contact angle measurements support the analysis of the SEM images. It demonstrates that the FSK modulation allows to change the surface wettability over a very broad range using the same precursor, the same discharge mode and configuration.

The third set of experiment is done with the conditions where the substrate are super-hydrophobic (f_{FSK} = 200 Hz and DC = 20%), varying the low frequency.

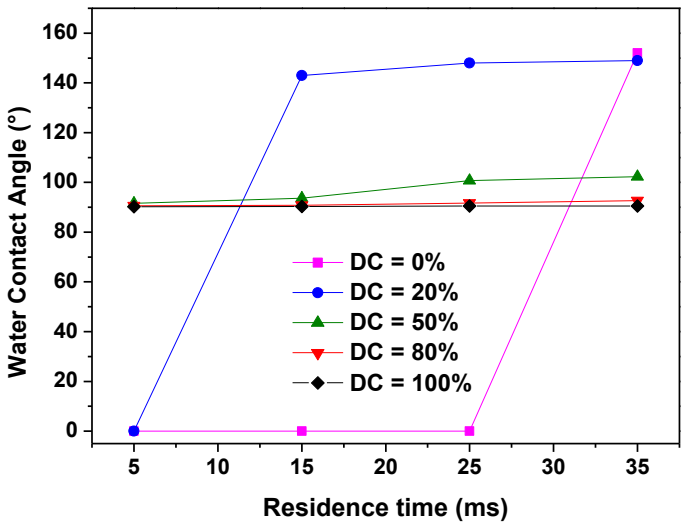

Figure 6: Water contact angle for a DC = 0% (square), DC = 20% (circle), DC = 50% (up-pointing triangle), DC = 80% (down-pointing triangle) and DC = 100% which represent IPA alone (Hexagon) as a function of the position in the plasma.

The aim of using a third set of parameters is to study how the oscillation amplitude of the NPs aggregates varies. The DC is set to 20%, for which the surface is not fully NP covered at the 1 kHz low frequency. Values of f_L lower (0.5 kHz) and higher (2 and 3 kHz) than 1 kHz are compared. The effect of this frequency on the surface coverage is very important with 100% being reached at 0.5 kHz even though the low frequency is applied three times less than at 1 kHz. On the other hand, an increase of the low frequency reduces drastically the surface coverage (Figures 5 and 7). As illustrated in Figure 6, for f_L of 1, 2 and 3 kHz, a large variation of the size distribution of the NPs aggregates on the surface occurs. The higher is the low frequency, the

smaller are the aggregates observed on the surface. This can easily be explained by the dependence of the particles oscillation amplitude on the sinusoidal voltage. The oscillation amplitude is proportional to the mobility of the particles and inversely proportional to the frequency.[24] Therefore, at a given frequency, the particles with a higher mobility (small NPs) have a longer oscillation amplitude and consequently a better chance to reach the substrate. In the range of f_L considered, the oscillation amplitude of the NPs aggregates varies significantly as compared to the gas gap. It thus plays the role of a size filter until the oscillations of the largest NPs aggregates are equal or larger than the gas gap.

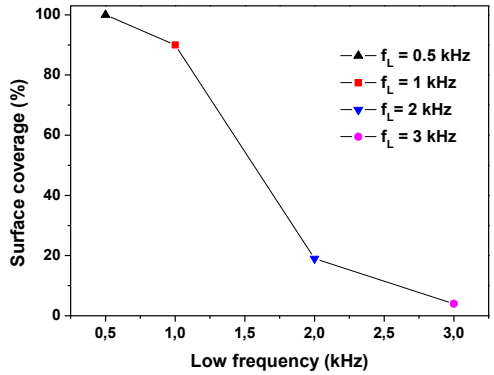

Figure 7: Average surface coverage of the substrate by the NPs as a function of the low frequency f_L value, $f_L = 0.5$ kHz (up-pointing triangle), $f_L = 1$ kHz (square), $f_L = 2$ kHz (down-pointing triangle) and $f_L = 3$ kHz (circle).

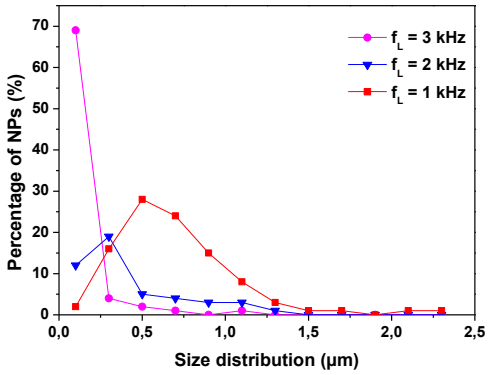

Figure 8 Percentage of NPs deposited as a function of their size for $f_L = 1$ kHz (square), $f_L = 2$ kHz (down-pointing triangle) and $f_L = 3$ kHz (circle).

3.2 Effect of parameters on the matrix deposition

The SEM image of the thin film cross-section provides the thickness of both NPs and matrix. For a DC of 0%, no matrix is deposited and only a thick but porous layer of NPs is observed. The absence of thin film polymerization is in agreement with the clearly observed 20 nm structure of the aggregates reported above. Even in the gas bulk, no IPA polymerization occurs which confirms that the polymerization rate is power-limited. Increasing the DC and thus the 15 kHz discharge power results in a thicker and thicker matrix while the NPs concentration decreases to almost zero for a DC of 100%. Figure 9 shows the average growth rate of the thick layer determined from the SEM cross-section as a function of the discharge power P_{FSK} and of the power during the 15 kHz duration of the FSK cycle, $P_{FSK\text{-}fH}$ for all the experiments (see Tables 1 and 2).

In Figure 9, for f_L = 1 kHz (set 1 and 2), three trends clearly appear. Up to $P_{FSK\text{-}fH}$ = 0.1 W.cm^{-2}, no coating is observed, which means that the power is too low to efficiently dissociate IPA. Thus, in these conditions, one can consider that IPA is not affected by the plasma (like it would be with the plasma off) and that it is transported farther in the plasma by the gas flow. Between 0.1 and 0.43 W.cm^{-2}, the average growth rate varies linearly with the discharge power and saturates beyond. This saturation can be explained by the large number of nanoparticles trapped in the discharge when the duty cycle is high, i.e. when the high frequency duration is long. As the quantity of NPs aggregates in the gas bulk increases, the consumption of the radicals by the NPs in the gas bulk is enhanced. The NPs aggregates are coated quicker than the delay required by the radicals to diffuse to the surface. This observation is in agreement with the results of a previous study where the growth rate of films synthesized with IPA and IPA+TiO_2 are compared.[10] In this case, a single frequency is used and the power varied by changing this frequency from 1 kHz to 50 kHz with a 50% amplitude modulation to ensure full surface

coating. The observed matrix growth rates are reported in Figure 9 (stars for IPA and hexagons for IPA+TiO_2) for comparison with the present results. The threshold at about 0.1 $W.cm^{-2}$ is also observed together with the linear increase. The slope is slightly lower when NPs are injected, which is attributed to the radical consumption by the NPs in the gas bulk. The similarity between these results and those obtained in the FSK mode for the 1 kHz low frequency is remarkable when considering the power of the 15 kHz DBD $P_{FSK\text{-}fH}$ rather than the total power P_{FSK}. This emphasizes that operating with a low frequency of 1 kHz is equivalent to operating with the discharge off for the deposition of the matrix as this frequency leads to a negligible IPA dissociation rate. To summarize, with the FSK voltage, even if the plasma is always on, from the IPA and NPs point of view, it plays the same role as a double amplitude modulation because the IPA is not (or is slightly) decomposed by the low frequency plasma. IPA is transported farther in the plasma when the low frequency is applied to ensure a high concentration of IPA everywhere in the plasma. The NPs behave similarly. They are trapped in the gas when the frequency is high, i.e. they are not affected by the electrical field and they are transported farther in the plasma by the gas flow. However, this observation remains true as far as the power of the low frequency discharge is smaller than 0.1 $W.cm^{-2}$ corresponding to the minimum value allowing the polymerization of IPA in the plasma. As reported by the full up-pointing triangle in Figure 9 for the third set of experiments, the high frequency power is constant and equal to 0.13 $W.cm^{-2}$ while the average growth rate varies from 1 to 15 $nm.min^{-1}$. This means that the high frequency power is not solely responsible of IPA decomposition. The increase of the low frequency from 1 to 3 kHz leads to an increase of the low frequency power from 0.12 to 0.36 $W.cm^{-2}$ (Table 1). These values are greater than the IPA polymerization power threshold so that they yield decomposition. In this case, the power that needs to be considered to evaluate the growth rate is

not limited to the high frequency power but is rather the sum of the high and low frequency powers, P_{FSK}, as represented by the open symbols in Figure 9.

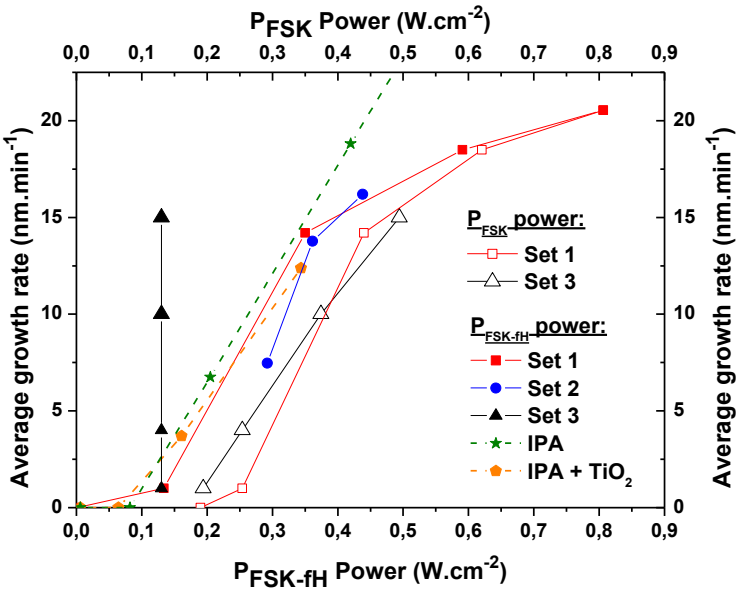

Figure 9: Full symbols, average growth rate as a function of the power when the high frequency is applied with power $P_{FSK\text{-}fH}$. The data were obtained for the first set (square), second set (circle), third set (up-pointing triangle) of conditions, for IPA alone (star) and for IPA+TiO_2 (hexagon). Open symbols, average growth rate as a function of the sum of high and low frequencies power P_{FSK}, first set (open square) and third set (up-pointing open triangle).

At 3 kHz, the matrix growth rate reaches more than 15 $nm.min^{-1}$ and the size of the NPs deposited are lower than 250 nm as reported in Figure 8. In this condition, as it is shown in Figure10, it's possible to deposited a nanocomposite thin film.

In that sense, the nanocomposite thin film deposited take benefits of the realization of a NPs size filter and a sufficient matrix growth rate with the FSK modulation f_{FSK} = 200 Hz, f_{fH} = 15 kHz,

f_{fL} = 3 kHz and DC = 20% by only using the DBD parameters and without acting in the suspension itself (functionalization).

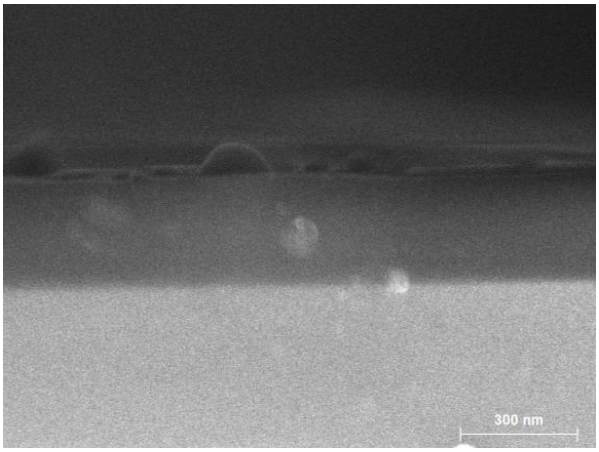

Figure 10: SEM cross-section of the nanocomposite deposited with f_{FSK} = 200 Hz, f_{fH} = 15 kHz, f_{fL} = 3 kHz and DC = 20%.

4. CONCLUSION

A FSK driven filamentary DBD is used to control the NPs content in the matrix for a composite thin film grown from a suspension of TiO_2 NPs in isopropanol, a polymerizable liquid. The interest of the FSK mode is that it easily allows to modulate two frequencies simultaneously. SEM images and wettability measurements show that the FSK voltage controls the NPs density and the matrix thickness. By only applying a low percentage (20%) of high frequency, the coating changes from superhydrophilic to superhydrophobic, taking benefit of the high surface roughness of the as-deposited NPs and of the IPA polymerization. The FSK mode should alternate two sinusoidal voltages over a time scale shorter but close to the gas residence time in the plasma. The voltage of the lower frequency should allow a significant oscillation of the

particles as compared to the gas gap while that of the higher frequency should be high enough to ensure the significant polymerization of the liquid. Moreover, increasing the low frequency can be beneficial because it helps to select NPs of small size on the substrate and to increase the power discharge during the low frequency so that IPA polymerization is facilitated. Finally, varying the duty cycle of the two frequencies, a feature easy to achieve and to precisely monitor in the FSK mode, allows to control the NPs content in the matrix and to realize a nanocomposite thin film.

AUTHOR INFORMATION

Corresponding Authors

E-mail: francoise.massines@pomes.cnrs.fr

E-mail: chaker@emt.inrs.ca

ACKNOWLEDGEMENTS. This work was funded by the "Agence Nationale de la Recherche" (project ANR -11- IS09 -0005) and by the National Science and Engineering Research Council (NSERC) of Canada. The authors are grateful to Emmanuel Hernandez from PROMES-CNRS and Etienne Charette from INRS-EMT for their technical involvement in the development of the DBD reactor and for their useful suggestions during the experiments.

References

1. Palgrave, R. G.; Parkin, I. P., Aerosol Assisted Chemical Vapor Deposition Using Nanoparticle Precursors: A Route to Nanocomposite Thin Films. *JACS* **2006,** *128* (5), 1587-1597.
2. Ward, L. J.; Schofield, W. C. E.; Badyal, J. P. S.; Goodwin, A. J.; Merlin, P. J., Atmospheric Pressure Glow Discharge Deposition of Polysiloxane and SiOx Films. *Langmuir* **2003,** *19* (6), 2110-2114.
3. Bardon, J.; Bour, J.; Del Frari, D.; Arnoult, C.; Ruch, D., Dispersion of Cerium-Based Nanoparticles in an Organosilicon Plasma Polymerized Coating: Effect on Corrosion Protection. *Plasma Process Polym* **2009,** *6*, S655-S659.
4. Fanelli, F.; Mastrangelo, A. M.; De Vietro, N.; Fracassi, F., Preparation of Multifunctional Superhydrophobic Nanocomposite Coatings by Aerosol-Assisted Atmospheric Cold Plasma Deposition. *Nanoscience and Nanotechnology Letters* **2015,** *7* (1), 84-88.
5. Fanelli, F.; Mastrangelo, A. M.; Fracassi, F., Aerosol-Assisted Atmospheric Cold Plasma Deposition and Characterization of Superhydrophobic Organic-Inorganic Nanocomposite Thin Films. *Langmuir* **2014,** *30* (3), 857-865.
6. Profili, J.; Levasseur, O.; Blaisot, J.-B.; Koronai, A.; Stafford, L.; Gherardi, N., Nebulization of Nanocolloidal Suspensions for the Growth of Nanocomposite Coatings in Dielectric Barrier Discharges. *Plasma Process Polym* **2016**, n/a-n/a.
7. Denis, D. P.; Barry, T.; Gerry, B., Effect of Titanium Oxide Nanoparticle Incorporation into nm Thick Coatings Deposited Using an Atmospheric Pressure Plasma. *Journal of Nanoscience and Nanotechnology* **2010,** *10* (4), 2746-2752.
8. Brunet, P.; Rincón, R.; Margot, J.; Massines, F.; Chaker, M., Deposition of homogeneous carbon-TiO_2 composites by atmospheric pressure DBD. *Plasma Process Polym* **2016**, n/a-n/a.
9. Profili, J.; Levasseur, O.; Naudé, N.; Chaneac, C.; Stafford, L.; Gherardi, N., Influence of the voltage waveform during nanocomposite layer deposition by aerosol-assisted atmospheric pressure Townsend discharge. *J. Appl. Phys.* **2016,** *120* (5), 053302.
10. Brunet, P.; Rincón, R.; Martinez, J.-M.; Matouk, Z.; Fanelli, F.; Chaker, M.; Massines, F., Control of composite thin film made in an Ar/isopropanol/TiO_2 nanoparticles Dielectric Barrier Discharge by the excitation frequency. *Plasma Process Polym* **2017**.
11. Martin, S.; Massines, F.; Gherardi, N.; Jimenez, C., Atmospheric pressure PE-CVD of silicon based coatings using a glow dielectric barrier discharge. *Surf. Coating Tech.* **2004,** *177*, 693-698.
12. Jidenko, N.; Jimenez, C.; Massines, F.; Borra, J. P., Nano-particle size-dependent charging and electro-deposition in dielectric barrier discharges at atmospheric pressure for thin SiOx film deposition. *J. Phys. D: Appl. Phys* **2007,** *40* (14), 4155-4163.
13. Borra, J. P., Nucleation and aerosol processing in atmospheric pressure electrical discharges: powders production, coatings and filtration. *J. Phys. D: Appl. Phys* **2006,** *39* (2), R19-R54.
14. Watson, S.; Nisol, B.; Lerouge, S.; Wertheimer, M. R., Energetics of Molecular Excitation, Fragmentation, and Polymerization in a Dielectric Barrier Discharge with Argon Carrier Gas. *Langmuir* **2015,** *31* (37), 10125-10129.
15. Bazinette, R.; Subileau, R.; Paillol, J.; Massines, F., Identification of the different diffuse dielectric barrier discharges obtained between 50 kHz to 9 MHz in Ar/NH3at atmospheric pressure. *Plasma Sources Sci. Technol.* **2014,** *23* (3), 035008.
16. Kogelschatz, U.; Eliasson, B.; Egli, W., Dielectric-barrier discharges. Principle and applications. *J. Phys. IV* **1997,** *7* (C4), 47-66.

17. Fanelli, F.; Fracassi, F., Aerosol-Assisted Atmospheric Pressure Cold Plasma Deposition of Organic–Inorganic Nanocomposite Coatings. *Plasma Chem. Plasma Process.* **2014,** *34* (3), 473-487.
18. Kasper, G., Electrostatic dispersion of homopolar charged aerosols. *Journal of Colloid and Interface Science* **1981,** *81* (1), 32-40.
19. Sarra-Bournet, C.; Ayotte, G.; Turgeon, S.; Massines, F.; Laroche, G., Effects of Chemical Composition and the Addition of H-2 in a N-2 Atmospheric Pressure Dielectric Barrier Discharge on Polymer Surface Functionalization. *Langmuir* **2009,** *25* (16), 9432-9440.
20. Gao, L.; McCarthy, T. J., The "Lotus Effect" Explained: Two Reasons Why Two Length Scales of Topography Are Important. *Langmuir* **2006,** *22* (7), 2966-2967.
21. Manca, M.; Cannavale, A.; De Marco, L.; Aricò, A. S.; Cingolani, R.; Gigli, G., Durable Superhydrophobic and Antireflective Surfaces by Trimethylsilanized Silica Nanoparticles-Based Sol−Gel Processing. *Langmuir* **2009,** *25* (11), 6357-6362.
22. Manoudis, P. N.; Karapanagiotis, I.; Tsakalof, A.; Zuburtikudis, I.; Panayiotou, C., Superhydrophobic Composite Films Produced on Various Substrates. *Langmuir* **2008,** *24* (19), 11225-11232.
23. Lee, S. G.; Ham, D. S.; Lee, D. Y.; Bong, H.; Cho, K., Transparent Superhydrophobic/Translucent Superamphiphobic Coatings Based on Silica–Fluoropolymer Hybrid Nanoparticles. *Langmuir* **2013,** *29* (48), 15051-15057.
24. Jidenko, N.; Borra, J. P., Kinematics of charged nanometric particles in silent discharges. *J. Phys. D: Appl. Phys.* **2005,** *38* (4), 617.